Role of DNA Flexibility in Sequence-Dependent Activity of Uracil DNA Glycosylase†

Eleanore Seibert,‡ J. B. Alexander Ross,*,‡,§ and Roman Osman*,||

Departments of Pharmacology and Biological Chemistry and of Physiology and Biophysics, Mount Sinai School of Medicine, One Gustave L. Levy Place, New York, New York 10029

Received May 13, 2002; Revised Manuscript Received July 3, 2002

ABSTRACT: Uracil DNA glycosylase (UDG) is a base excision repair enzyme that specifically recognizes and removes uracil from double- or single-stranded DNA. The efficiency of the enzyme depends on the DNA sequence surrounding the uracil. Crystal structures of UDG in complex with DNA reveal that the DNA is severely bent and distorted in the region of the uracil. This suggests that the sequence-dependent efficiency of the enzyme may be related to the energetic cost of DNA distortion in the process of specific damage recognition. To test this hypothesis, molecular dynamics simulations were performed on two sequences representing extreme cases of UDG efficiency, AUA/TAT (high efficiency) and GUG/CAC (low efficiency). Analysis of the simulations shows that the effective bending force constants are lower for the AUA/TAT sequence, indicating that this sequence is more flexible than the GUG/CAC sequence. Fluorescence lifetimes of the adenine analogue 2-aminopurine (2AP), replacing adenine opposite the uracil, are shorter in the context of the AUA/TAT sequence, indicating more dynamic base−base interaction and greater local flexibility than in the GUG/CAC sequence. Furthermore, the K_M of *Escherichia coli* UDG for the AUA/TAT sequence is 10-fold smaller than that for the GUG/CAC sequence, while the k_{cat} is only 2-fold smaller. This indicates that differences in UDG efficiency largely arise from differences in binding and not catalysis. These results link directly flexibility near the damaged DNA site with the efficiency of DNA repair.

Uracil arises in DNA[1] from misincorporation during DNA replication (A·U) or as a result of the spontaneous hydrolytic deamination of cytosine (G·U). While the A·U base pair is not directly mutagenic, some transcription factors have significantly reduced binding affinity for A·U compared to A·T base pairs (*1*), which can affect gene expression. Thus, although the eukaryotic replicative polymerases have a high fidelity, with misincorporation occurring at a rate of approximately 1×10^{-7} per base pair per generation (*2*), the finite probability presents undesired biological consequences. In humans, spontaneous deamination of cytosine occurs at a rate of approximately 100−500 events per cell per day (*3*). Failure to repair the G·U base pair leads to a G·C transition mutation to A·C during DNA replication. Consequently, the presence of uracil in DNA is detrimental, and its removal by repair enzymes is essential to normal cell function. This repair function is initiated by uracil DNA glycosylase (UDG), an enzyme of the base excision repair (BER) pathway (*4*, *5*), which is found in all prokaryotes and eukaryotes. UDG recognizes and removes uracil in U·A and U·G base pairs from both double- and single-stranded DNA (*6*, *7*).

UDG must be capable of recognizing its substrate, uracil, and discriminating it from thymine, which differs only by a methyl group on C5. The high specificity of UDG is due in part to an active site tyrosine (Tyr 147 in human UDG), which sterically excludes thymine as well as purines from entering the binding pocket (*8*−*10*). Hydrogen bonding between the uracil and an active site asparagine (Asn 204 in human UDG) provides selectivity between uracil and cytosine (*11*). Mutation of Tyr 147 to alanine, cysteine, or serine, or of Asn 204 to aspartic acid, produces a mutant UDG that catalyzes the removal of either thymine or cytosine, respectively. However, these mutant enzymes are still 1−2 orders of magnitude more selective for uracil than either cytosine or thymine (*12*). The high selectivity of the mutant enzymes for uracil suggests that other factors also contribute to the specificity of UDG.

Crystal structures have shown that DNA in complex with UDG is bent by about 40° and that the uracil is extrahelical. DNA bending is thought to occur via a "Ser-Pro pinch" mechanism, in which the DNA backbone is compressed by serine−proline-rich loops of UDG (*13*). Parikh and coworkers suggest that damaged sites along the DNA may

† This work was supported by USPHS Grant CA 63317. E.S. was supported by training grants GM08553 and CA78207. Preliminary results of this work were presented at the 45th Annual Meeting of the Biophysical Society (Boston, MA, 2001).

* To whom correspondence should be addressed. Tel: (406) 243-6026; (212) 241-5609. Fax: (212) 860-3369. E-mail: sandy@selway.umt.edu; osman@inka.mssm.edu.

‡ Department of Pharmacology and Biological Chemistry, Mount Sinai School of Medicine.

§ Current address: Department of Chemistry, University of Montana, Missoula, MT 59812.

|| Department of Physiology and Biophysics, Mount Sinai School of Medicine.

[1] Abbreviations: UDG, uracil DNA glycosylase; 2AP, 2-aminopurine; d2AP, 2-aminopurine deoxyribose; MD, molecular dynamics; DNA, deoxyribonucleic acid; *E. coli*, *Escherichia coli.*

10.1021/bi026121o CCC: $22.00
Published on Web 08/15/2002

allow greater compression than undamaged sites and that the combination of backbone compression and insertion of the Leu 272 side chain into the minor groove facilitates flipping of the uracil through the major groove.

Although energetically favorable contacts are made between UDG and the uracil base, the processes of DNA bending and base flipping are energetically unfavorable. Base flipping requires the loss of favorable stacking interactions between adjacent bases and the breakage of hydrogen bonds with the complementary base. Depending on the dinucleotide step, the energy of base stacking varies from approximately −3 to −5 kcal/mol in aqueous solution (*14*), while the free energy of hydrogen bonding has been estimated to be between −0.5 and −2 kcal/mol per hydrogen bond (*15*). When DNA is bent, the energy difference is reduced between the "flipped-out", or open, state and the "flipped-in", or closed, state (*16*). Thus, the relative stability of the open state is greater in the context of a bent DNA. In addition, recent molecular dynamics studies have demonstrated a coupling between DNA bending and base opening (*17*). Together with the structural data, these computational results suggest that highly flexible DNA sequences would be better substrates for UDG.

DNA flexibility is a sequence-dependent property (*18*). Accordingly, we expect that UDG activity would depend on the nucleotide sequence surrounding the uracil. While UDG recognizes and removes uracil in any sequence context, Slupphaug and co-workers have reported sequence-dependent variations of up to 20-fold in UDG efficiency for different DNA sequences for human (*19*), *Escherichia coli* (*E. coli*) (*20*), and bovine UDG (*21*). Attempts to correlate changes in UDG efficiency with changes in melting temperature of the differing sequences did not lead to a clear relationship, indicating that factors other than melting temperature may influence UDG activity for its substrate. A recent kinetic analysis on herpes simplex virus 1 (HSV1) UDG activity for various substrates showed that K_M varied approximately 6-fold, while k_{cat} varied only 1.5-fold, indicating that the sequence dependence results from differences in binding energy (*22*). The authors attributed the variations in binding energy to differences in local DNA structure surrounding the uracil.

The energetic penalty of distorting a flexible DNA sequence would be smaller than that of a rigid sequence. Thus, we hypothesize that sequences with greater local flexibility in the region of the uracil should be better substrates for UDG. This hypothesis is consistent with reports showing that single-stranded DNA, which is more flexible than double-stranded DNA, binds with higher affinity to UDG (*23*) and also is a better substrate (*19*). To test this hypothesis, we have chosen two sequences with extremely high and low UDG efficiency, as reported previously by Slupphaug et al. (*19*) (see Table 1). We have adopted a combined theoretical/experimental approach to determine the variations in local DNA flexibility of these sequences and to study the effect of these differences on the kinetic constants of uracil removal by UDG. This work involves several stages. In the first stage, molecular dynamics simulations are used to probe local differences in the structural and dynamical properties of each sequence in order to develop a model of DNA flexibility. Second, we take advantage of a recently developed method of determining local DNA flexibility that utilizes fluorescence spectroscopy of the fluorescent adenine analogue 2-aminopurine (2AP). Analysis of fluorescence lifetime data and quantum yields allows an assessment of local dynamics and base stacking interactions, demonstrating an agreement between conclusions from the fluorescence data and the MD simulations. Finally, our hypothesis regarding the role of DNA flexibility in enzyme−DNA interaction is tested with kinetic assays on each sequence.

Table 1: DNA Oligonucleotide Sequences

name[a]	sequence						
	Simulation (11-mers)						
A**U**A[b]/T**A**T	5′-A_1AG	CA**U**$_6$	AAA	GT_{11}	-3′		
	3′-T_{22}TC	GT**A**$_{17}$	TTT	CA_{12}	-5′		
G**U**G/C**A**C	5′-C_1AG	GG**U**$_6$	GGT	TT_{11}	-3′		
	3′-G_{22}TC	CC**A**$_{17}$	CCA	AA_{12}	-5′		
	Experiment (19-mers)						
A**U**A/T**P**T[c]	5′-CCG	GAA	GCA	**U**AA	AGT	GCG	C-3′
	3′-GGC	CTT	CGT	**P**TT	TCA	CGC	G-5′
G**U**G/C**P**C	5′-CCG	GCA	GGG	**U**GG	TTT	GCG	C-3′
	3′-GGC	CGT	CCC	**P**CC	AAA	CGC	G-5′

[a] The oligos are named with the upper strand in the 5′ to 3′ direction and the lower strand in the 3′ to 5′ direction. [b] U represents deoxyuridine. [c] P represents 2-aminopurine.

MATERIALS AND METHODS

Computational Methods. Initial DNA 11-mer structures with the sequences shown in Table 1 were generated in the B-DNA conformation using the Nucgen module of AMBER 6.0 (*24*). The DNA was solvated in a periodic box of TIP3P waters, and 20 Na^+ ions were included to neutralize the charge on the phosphates. First, the water and counterions were minimized with the DNA immobilized. Subsequently, the energy of the entire system including the DNA was minimized. The system was heated to 300 K over 2 ps, with positional restraints of 500 kcal/Å^2 on the DNA, which were gradually reduced by a factor of 2 every 2 ps, while the system was held at constant temperature (300 K). Equilibration was completed by running molecular dynamics on the unrestrained system for 20 ps. During this time, the density, energy, volume, and temperature achieved stability. The density was equilibrated under constant pressure to a value of 1.035 g/cm^3, which resulted in a box size of approximately $47 \times 44 \times 61$ Å^3. Production molecular dynamics simulations of 5 ns then were carried out under conditions of constant pressure and temperature (300 K) with a time step of 2 fs using the Sander module of AMBER 6.0 (*24*). Snapshots were written to the trajectory every 0.2 ps.

DNA bending analysis was performed using CURVES (*25*). The parameters A_{tip} (bending toward grooves) and A_{inc} (bending toward backbone) at the U_6-A_{17} step (see Table 1) were calculated for each snapshot in the trajectory. Two-dimensional histograms were prepared by binning the values of A_{tip} and A_{inc} into 2° square bins (see Figure 1). These distributions were transformed into energy surfaces using a potential of mean force (PMF) approach. The work required to go from point x_0y_0 to x_1y_1 on the surface is calculated as

$$\Delta\omega(x_0y_0 \rightarrow x_1y_1) = -RT\ln(N_{x_1y_1}/N_{x_0y_0}) + \omega_0 \qquad (1)$$

where $N(x_0y_0)$ is the maximum of the distribution and ω_0 is

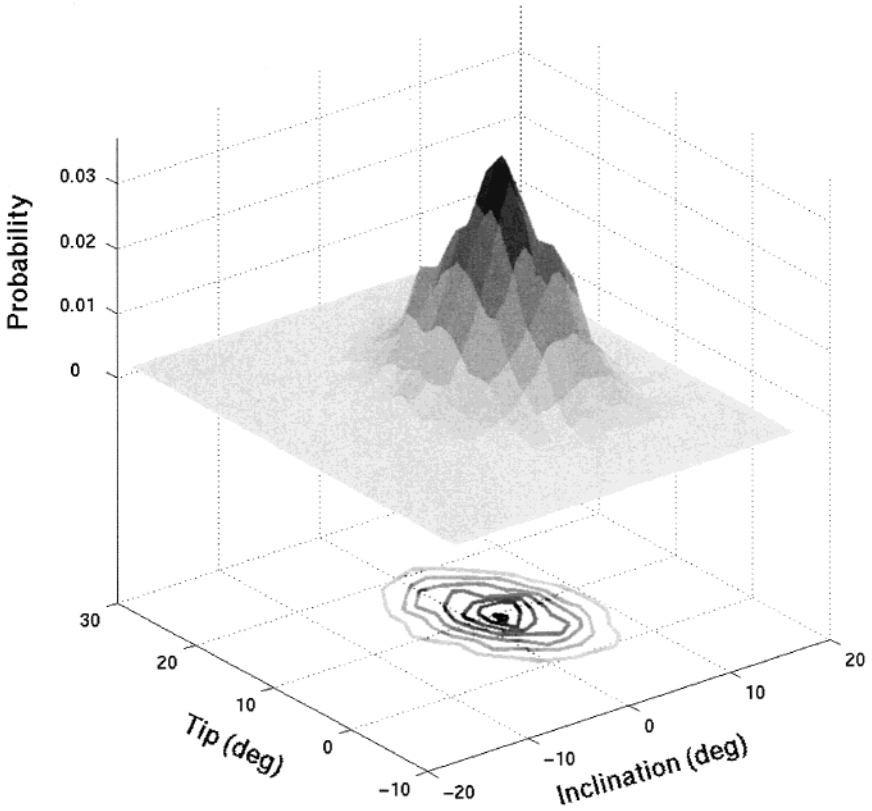

FIGURE 1: Representative two-dimensional probability histogram for bending in each direction. Contour lines are shown below the surface.

an integration constant, which has been set to zero for the (x_0, y_0) position. Gnuplot 3.7 was utilized to fit the PMF surface to a two-dimensional polynomial with weighting factors such that the more populated bins are weighted more heavily:

$$\sigma_i = kT/\sqrt{N_{x_i y_i}} \tag{2}$$

Force constants were obtained as partial second derivatives with respect to A_{tip} and A_{inc} at the minimum of the energy surface. The harmonic mean force constant (k_H), which assumes the DNA to be an isotropic rod, was calculated according to

$$k_H = 2k_{tip}k_{inc}/(k_{tip} + k_{inc}) \tag{3}$$

Oligonucleotides. All experiments were performed on 19-mer oligonucleotides, since losses were substantially less during dialysis and concentration as compared to 11-mers. Furthermore, double-stranded DNA 19-mers have previously been shown to be thermodynamically stable at the temperatures used in our experiments (*26*). Oligonucleotides containing either uracil or 2AP were ordered from Oligos Etc. (Bethel, ME). The single-stranded 19-mer oligos were purified on a MonoQ 5/5 ion-exchange resin (Pharmacia) using a linear gradient of NaCl (0−1 M) in 10 mM Tris-HCl and 1 mM Na_2EDTA, pH 8.0. For annealing, a 5% molar excess of the uracil-containing strand was included, such that all 2AP-containing strands were present in double-stranded form. Annealing was performed by heating complementary strands to 90 °C for 5 min and gradually cooling them to room temperature. The double-stranded oligos were purified from single-stranded material using the MonoQ column and a linear gradient of NaCl (0−1 M) in the buffer described above. Oligo concentrations were determined from absorbance spectroscopy, assuming the extinction coefficient of 2AP to be $\epsilon_{303nm} = 6000\ M^{-1}\ cm^{-1}$ (*27*).

Spectroscopy. Absorption spectra were measured using a dual-beam U-3210 Hitachi spectrophotometer. Steady-state fluorescence spectroscopy was carried out using an SLM 4800 spectrofluorometer modified in the laboratory for single-photon counting. Fluorescence emission spectra were obtained by exciting 2AP at 325 nm to avoid the absorption of the natural DNA bases. Band-passes of 4 and 8 nm were used for excitation and emission, respectively. Time-resolved fluorescence decay curves were collected using a time-correlated, single-photon counting instrument that has been described previously (*28*). Sample lifetimes were measured in an automated sample chamber (Quantum Northwest: FLASC) with excitation at 305 nm, due to wavelength limitations of the laser, and emission was detected at 360 nm. Inner filter effects do not influence the fluorescence lifetime, and thus this excitation wavelength is not problematic. The instrument response function was measured using a dilute suspension of colloidal silica. Decay curves were collected into 4000 channels with a timing calibration of 10 ps per channel. Instrument response functions and sample intensity decay curves were collected to 100000 and 40000 peak counts, respectively.

Time-resolved fluorescence data were analyzed by a standard reconvolution (*29*) procedure using nonlinear regression (*30*). The fluorescence decay was fitted to a sum of exponentials:

$$I(t) = \sum \alpha_i e^{-t/\tau_i} \tag{4}$$

where α_i is the amplitude of each component and τ_i is the corresponding recovered fluorescence lifetime. Multiexponential decays were required to fit the decays of 2AP in DNA. The number-average lifetime, which represents the area under the decay curve, was calculated according to

$$\tau_{num} = \sum \alpha_i \tau_i / \sum \alpha_i \quad (5)$$

where the product $\alpha_i\tau_i$ is the intensity contribution of the *i*th component. Joint support plane confidence intervals were calculated for all iterated parameters by the approximation method described by Johnson and co-workers (*31*).

Contributions of static and dynamic quenching of 2AP in the oligos were calculated as described previously (*27*). As static quenching does not affect the fluorescence lifetime, the reduction in lifetime is assumed to be due to dynamic quenching. The fraction of 2AP statically quenched, f_{SQ}, is calculated as

$$f_{SQ} = 1 - \phi_{rel}/\tau_{rel} \quad (6)$$

where ϕ_{rel} and τ_{rel} represent the quantum yield and fluorescence lifetime relative to 2AP deoxyribose (d2AP), respectively.

UDG Purification and Activity Assays. E. coli UDG was purified as described previously (*32*), and the protein concentration was determined from absorbance spectroscopy using $\epsilon_{280nm} = 38500\ M^{-1}\ cm^{-1}$ (*27*). A fluorescence-based assay was used to determine the glycosylase activity (*32*). In this assay, the analogue 2AP is opposite uracil in the complementary strand, and upon cleavage of the glycosylic bond of the uracil by UDG, an increase in 2AP fluorescence is observed. Assays were carried out in 10 mM Tris-HCl, 20 mM NaCl, and 2.5 mM $MgCl_2$ at pH 8. 2AP was excited at 310 nm, and the increase in fluorescence as a function of time was observed at 370 nm. Reaction rates were calculated from the initial linear region of the assay curve as described (*32*). The observed rate divided by the concentration of the enzyme yielded an observed rate constant, k_{obs}, for each concentration of substrate. To determine k_{cat} and K_M, the dependence of k_{obs} on substrate concentration was fitted to

$$k_{obs} = k_{cat}[S]/(K_M + [S]) \quad (7)$$

where [S] is the concentration of uracil-containing DNA.

RESULTS AND DISCUSSION

Molecular dynamics (MD) simulations were carried out for 5 ns on the 11-mer DNA sequences shown in Table 1. These sequences were chosen because UDG efficiency reported by Slupphaug et al. (*19*) was approximately 20-fold greater for the oligonucleotide containing the AUA/TAT sequence compared to the one containing the GUG/CAC sequence. The simulations were stable as judged by root-mean-square deviation from the average structure (1.5 ± 0.3 Å), as well as by fluctuations in temperature (300 ± 2 K) and density (1.037 ± 0.002 g/cm^3).

The crystal structures of UDG in complex with DNA show that the DNA is bent in the region of the uracil, and thus we focused on this region for the analysis of the MD simulations. Bending of the DNA at the uracil toward the grooves and toward the backbone was calculated in CURVES (*25*) using the axis curvature parameters A_{tip} and A_{inc}. A potential of mean force approach was used to obtain effective local bending force constants in each direction, as described in Materials and Methods. A two-dimensional second-order polynomial did not provide good quality fits of the energy surface, as judged by χ^2, the weighted sum of squares of residuals. However, a two-dimensional third-order polynomial produced an acceptable χ^2, which did not improve significantly with the introduction of higher order terms. Bending force constants for the uracil with respect to its 3′ and 5′ neighbors were calculated by taking the second derivative of the fitted PMF at its minimum. The force constants for bending in each direction as well as harmonic mean force constants are presented in Table 2. At both base pair steps with uracil in the 3′ or 5′ position in relation to the adjacent purine (A or G), the bending force constants are smaller for the AUA/TAT sequence than for the GUG/CAC sequence. This is true for the individual force constants of bending toward the groove (K_{tip}) and bending toward the backbone (K_{inc}), as well as for the harmonic bending force constants. Hence, the AUA/TAT sequence is locally more flexible, or easily bent, in the region of the uracil than the GUG/CAC sequence. The force constant analysis also provides information about the anisotropy of DNA bending, which is a measure of the differential DNA flexibility with respect to each of its axes. The deviation from zero (isotropic rod) is a measure of the anisotropy and reflects the fact that the force constants for bending toward the groove in each sequence (Table 2) are approximately two times smaller than those for bending toward the backbone. The bending anisotropy can be observed for a representative distribution in Figure 1, since the distribution is broader along the tip axis (bending toward grooves). Lankaš and co-workers reported similar trends in force constants for trimer segments of simulated DNA oligomers (*33*). The ratios of force constants obtained by these two similar methods are in close agreement, which implies that the observed local bending anisotropy is an inherent characteristic of DNA and is not biased by the method of determining the force constants.

Table 2: Force Constants for Bending in the Region of the Uracil

	k_{bend} (kcal/rad^2)			
sequence[a]	tip	inclination	harmonic mean	anisotropy[b]
AUA/**TA**T	62	149	88	0.41
A**UA**/T**AT**	63	141	87	0.39
GUG/**CA**C	72	180	103	0.40
G**UG**/C**AC**	69	159	96	0.25

[a] Letters in boldface represent the specific base pair step that has been analyzed. [b] Bending anisotropy was calculated according to the equation $A = (k_{inc} - k_{tip})/(k_{inc} + k_{tip})$.

The analysis of bending force constants indicates that the DNA in the region of the uracil in the A·T context is more flexible than in the G·C context. However, this analysis is limited to bending and does not provide a measure of other degrees of freedom that contribute to local flexibility. A variety of experimental methods, including gel cyclization and gel mobility retardation, have been used to quantitate DNA flexibility (*34*, *35*). Whereas these methods provide a measure of *overall* DNA distortion and flexibility, we are interested in the *local* flexibility in the region of the uracil. We have recently reported a method using the fluorescent nucleotide analogue 2AP (*27*) that is sensitive to changes in

Table 3: Intensity Decay Parameters for 2AP in the Oligonucleotides

oligo	τ_1 (ns)	τ_2 (ns)	τ_3 (ns)	α_1	α_2	α_3
AUA/TPT	0.20 (0.196, 0.205)[a]	0.39 (0.384, 0.394)	6.8 (4.911, 9.150)	0.49 (0.465, 0.511)	0.51 (0.491, 0.520)	0.003 (0.003, 0.003)
GUG/CPC	0.43 (0.406, 0.459)	1.7 (1.669, 1.709)	7.4 (7.317, 7.432)	0.31 (0.291, 0.336)	0.48 (0.476, 0.491)	0.21 (0.203, 0.208)

[a] Values in parentheses represent 95% confidence limits.

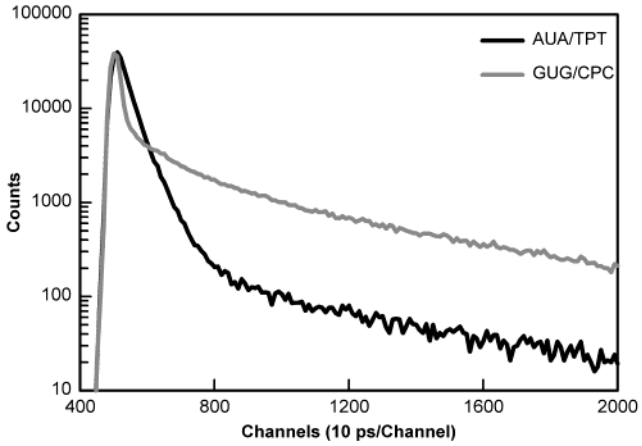

FIGURE 2: Time-resolved decay curves of 2-aminopurine opposite uracil in two sequence contexts.

the local conformation and dynamics of the DNA in the vicinity of the probe.

The observed fluorescence lifetime of 2AP is reduced due to collisions with a quencher molecule during the excited-state lifetime. In solution, all four bases that occur naturally in DNA are highly efficient collisional (dynamic) quenchers of 2AP fluorescence (*28*). On this basis, collisions between 2AP and the 3′ or 5′ bases in DNA would be expected to decrease the fluorescence lifetime. We have demonstrated previously that the average fluorescence lifetime of 2AP is shorter in flexible sequences as compared to rigid sequences (*27*). Furthermore, the quantum yield of 2AP fluorescence in DNA shows greater reduction than does the lifetime. Purely collisional quenching results in a proportionate decrease in quantum yield and fluorescence lifetime, and a larger decrease in the quantum yield relative to that of the lifetime indicates the presence of static quenching. We have demonstrated that the naturally occurring DNA bases not only act as efficient collisional quenchers of 2AP fluorescence but also participate in static quenching through intermolecular association in the ground state (*28*). Thus, the static quenching in DNA reflects stacking interactions between 2AP and the adjacent 3′ or 5′ bases (*27*).

Oligos were designed with 2AP opposite uracil to allow measurement of the local dynamics of the DNA in this region. Fluorescence decay curves are shown for each oligo in Figure 2. Clearly, the shape of the fluorescence decay profile of 2AP differs dramatically between the two sequences. A single exponential did not adequately describe the fluorescence intensity decay data for either sequence, and thus the fluorescence decay curves were analyzed as a sum of exponentials (eq 4). Three components were required to obtain acceptable values of χ^2 and randomly distributed residuals. The fluorescence amplitudes and lifetimes are presented in Table 3. A long lifetime component of approximately 7 ns is observed in both sequence contexts.

Table 4: Relative Quantum Yields and Number-Average Lifetimes for 2AP in the Oligonucleotides

sample	ϕ_{rel}	τ_{num} (ns)	τ_{rel}/ϕ_{rel}	f_{SQ}
d2AP	1[a]	10.2	1	0
A**U**A/T**P**T	0.017	0.32	1.88	0.47
G**U**G/C**P**C	0.0013	2.48	184.52	0.99

[a] Relative quantum yield of d2AP is taken to be 1 by definition.

However, in the AUA/TPT context, this lifetime has a very small preexponential factor. Approximately 93% of the fluorescence intensity of 2AP in the AUA/TPT context is accounted for by the two short lifetimes below 1 ns, indicating that 2AP in this sequence context undergoes efficient collisional quenching. In the GUG/CPC context, the individual lifetimes are longer than in the AUA/TPT context, and the contribution of the short lifetime component to the total fluorescence intensity is only 5%. We have greater confidence in the average fluorescence lifetime as compared to the individual lifetime components, because it does not suffer from the problem of correlation between the lifetimes (τ) and preexponential factors (α) during the fitting process. The average lifetimes of 2AP in each sequence context, reported in Table 4, clearly illustrate the differences between the two sequences. The average lifetime, τ_{num}, is 0.32 ns in the AUA/TPT sequence and 2.48 ns in the GUG/CPC sequence (Table 4). These results suggest that the frequency of collision of 2AP with its neighbors in the GUG/CPC context is considerably less in the AUA/TPT context. Thus, the AUA/TPT sequence is locally more flexible than the GUG/CPC sequence. This observation is in agreement with the results of our MD simulations, which show that the AUA/TAT sequence is locally easier to bend than the GUG/CAC sequence.

To characterize the degree of stacking of the DNA in the region of the uracil, we measured relative quantum yields for each oligo. A combination of steady-state and time-resolved fluorescence spectroscopy enables the separation of dynamic quenching (DNA flexibility) and static quenching (stacking interactions) (*27*). Fluorescence emission spectra for each oligo are shown in Figure 3. A dramatic difference in the fluorescence quantum yield between the two oligos is observed. The quantum yield of 2AP in the AUA/TPT context is approximately 12.5 times larger than that of 2AP in the GUG/CPC context. The relative quantum yields and relative lifetimes compared to 2-aminopurine deoxyribose (d2AP), as well as the fraction statically quenched, f_{SQ}, calculated according to eq 6, are presented in Table 4. In the more flexible AUA/TPT context about half of the 2AP is statically quenched; emission is observed for 53% of the molecules. By contrast, in the GUG/CPC context 99% of the 2AP is statically quenched, presumably due to stacking interactions, and fluorescence emission is observed only in approximately 1% of the 2AP. Thus, it appears that stacking contributes to increased rigidity.

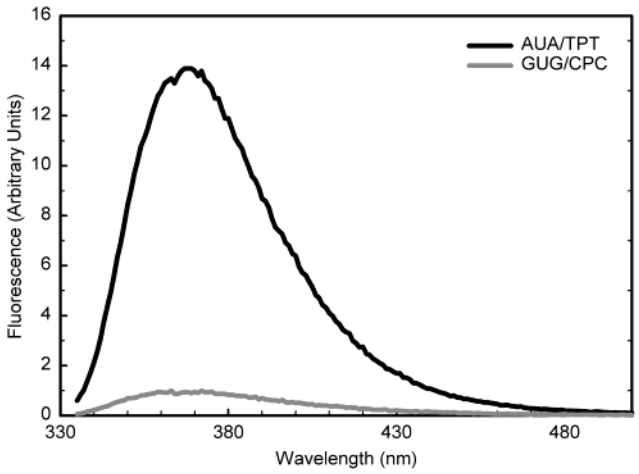

FIGURE 3: Fluorescence emission spectra for 2-aminopurine in each sequence context.

We would like to understand the molecular basis for the differences in fluorescence quenching of 2AP in the two sequence contexts. Since quenching, both dynamic and static, can arise through collisions and interactions with neighboring bases, we compared the distributions of the six interbase parameters (shift, slide, rise, tilt, roll, and twist) that describe the translations and rotations of adjacent bases. The adenine opposite the uracil was studied since its position within the DNA in the MD simulations corresponds to the adenine analogue, 2AP, used in the fluorescence experiments. The widths of the distributions describing dynamic motions of adjacent bases relative to one another should correlate with collisional quenching. Distributions of the six interbase parameters are shown in Figure 4. On the 3′ side of the adenine that models the 2AP, the distributions of slide, rise, tilt, roll, and twist are narrower for the AUA/T**A**T sequence than for the GUG/C**A**C sequence (Figure 4A). Only shift is narrower for the GUG/C**A**C sequence. Thus, the distributions of the interbase parameters on the 3′ side of the adenine do not correlate with the dynamic quenching results for 2AP. In contrast, on the 5′ side of the adenine, the distributions of shift, rise, and tilt are broader for the AUA/T**A**T sequence (Figure 4B). This suggests that the collisions between the 5′ neighboring base to 2AP are more effective in quenching the excited state than those on the 3′ side. The quantum chemical calculations of Jean and Hall showed subtle

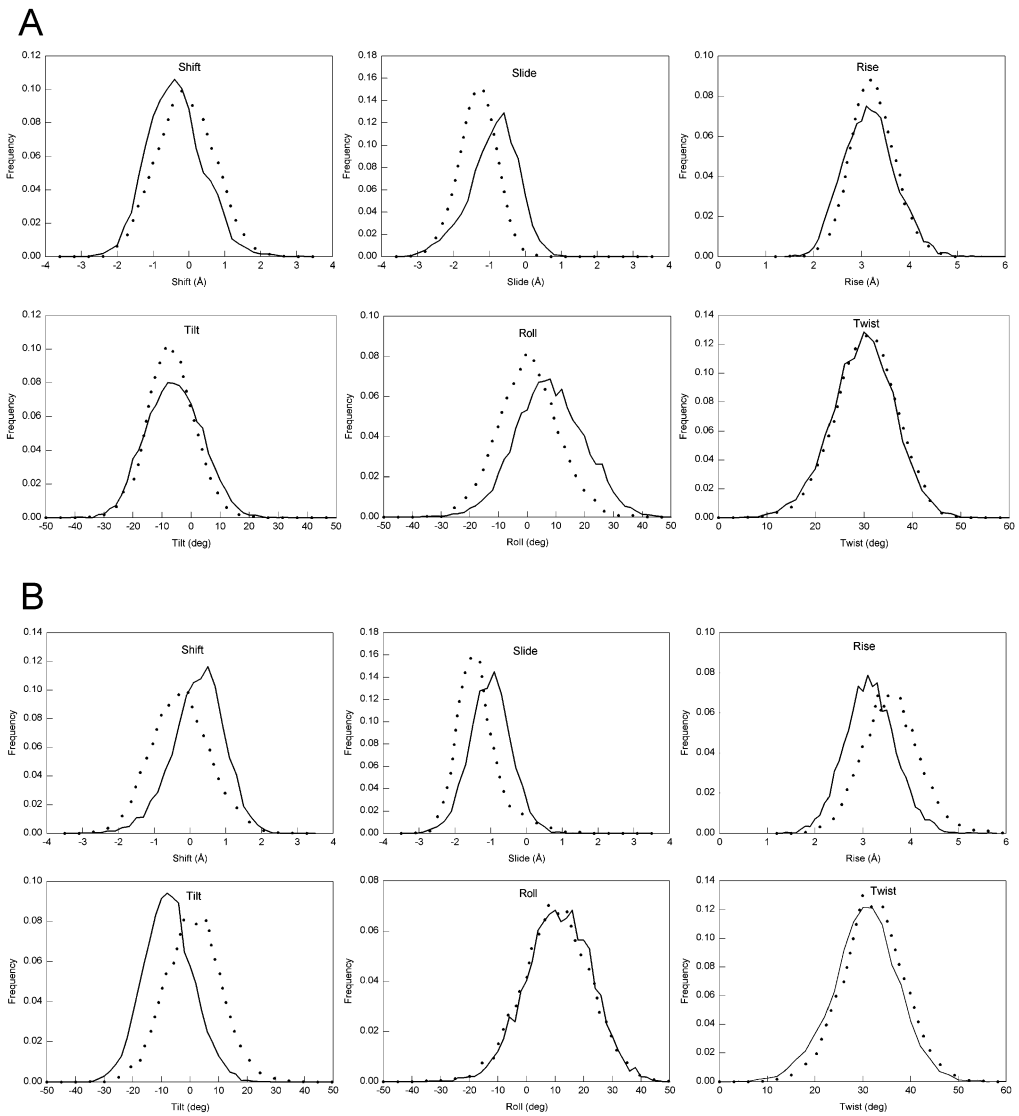

FIGURE 4: Distributions of interbase parameters measured between the adenine opposite the uracil and its 3′ (A) and 5′ (B) neighbors. Key: AUA/TAT (dashed line), GUG/CAC (solid line).

differences in the dynamic quenching of 2AP by thymine as 3′ and 5′ neighbors (*36*). Specifically, the energy gap between the "dark" S1 and the "bright" S2 excited states is significantly smaller for the case of 2AP with thymine on the 5′ side, suggesting that the 5′-thymine is a more efficient collisional quencher of 2AP fluorescence. This is in agreement with our prediction, based on the widths of the interbase parameter distributions, that the 5′ neighbor is a more efficient dynamic quencher than the 3′ neighbor.

Jean and Hall showed that static quenching is enhanced in A-form DNA as compared to B-form DNA (*36*). A-DNA is characterized by smaller rise and twist and larger slide and roll than B-DNA (*15*). These geometrical differences lead to greater overlap of the rings of neighboring bases for A-DNA as compared to B-DNA (*37*), which allows greater stacking of the bases. The distributions of the six local interbase parameters of the adenine opposite the uracil were utilized to interpret the static quenching data of our fluorescence experiments. The most probable geometry of the base pair step can be assessed from the positions of the maxima of the six interbase parameters distributions; these should correlate with the degree of static quenching. At the 5′ side of the adenine (Figure 4B), the average rise distance is 3.5 Å for the AUA/T**A**T sequence as compared to 3.1 Å for the GUG/C**A**C sequence, which is more similar to that of A-DNA [2.9 Å (*15*)]. Slide is greater at both the 5′ and 3′ sides for the GUG/C**A**C sequence, also consistent with its being locally more "A-DNA-like". Furthermore, the average roll of the adenine and its 3′ neighbor is larger and more A-DNA-like [6−9° (*15*)] for the GUG/C**A**C sequence (6.8°) as compared to the AUA/T**A**T sequence (−0.7°). Thus, the interbase parameters of the GUG/C**A**C are consistent with a geometry more similar to A-DNA, and greater stacking of the adenine is expected in this sequence context relative to the AUA/T**A**T context. The analysis of the interbase parameters is in agreement with experiment, which shows that 2AP is significantly more statically quenched (stacked) in the GUG/CPC context.

The results of the MD simulations and fluorescence spectroscopy demonstrate distinct differences in the structural properties of the two sequences, most notably differences in the maxima of the distributions of slide, rise, and roll. These differences consistently point to the involvement of enhanced stacking between cytosine and 2AP that leads to a dramatic reduction in quantum yield. Furthermore, clear differences in the dynamical properties of the sequences are observed, with wider distributions of shift, rise, and tilt on the 5′ side of the AUA/T**A**T sequence suggesting that more collisions of 2AP with its neighbors occur in this context as compared to the GUG/C**A**C context. The enhanced frequency of collision between thymine and 2AP leads to a reduction of the fluorescence lifetime in the AUA/TPT context. The greater flexibility of the AUA/TPT sequence reflected in the larger frequency of collisions suggests a molecular mechanism for the differential sequence-dependent UDG efficiency (*19*). The formation of the UDG−DNA complex involves distortion of the DNA as indicated by the crystal structures (*13*). Thus, the AUA/TPT oligo should be a better substrate for UDG, as it would require less energy to be distorted. This should be reflected in the binding step and not during the subsequent catalytic step. Hence, we would predict that the origin of the difference in enzyme efficiency for processing uracil is due to differences in K_M rather than in k_{cat} since binding should be tighter to the AUA/TPT oligo.

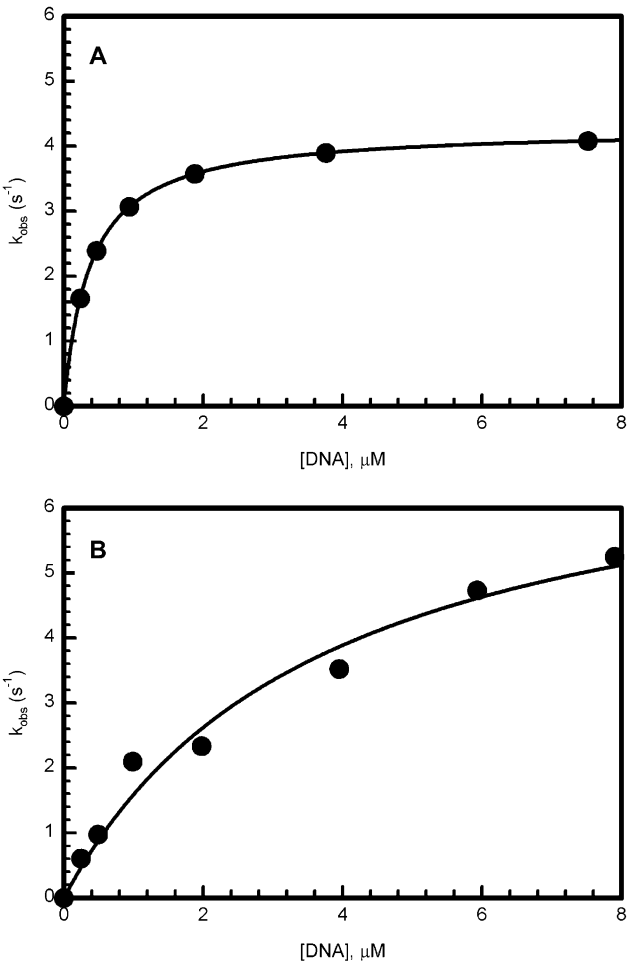

FIGURE 5: Kinetics of uracil removal for the AUA/TPT sequence (A) and the GUG/CPC sequence (B). Solid lines represent best fits through the data, assuming a Michaelis−Menten model.

Table 5: Kinetic Parameters of UDG Catalysis

sequence	K_M (μM)[a]	k_{cat} (s^{-1})
A**U**A/T**P**T	0.33 ± 0.11	4.3 ± 0.4
G**U**G/C**P**C	3.72 ± 2.50	7.5 ± 2.3

[a] Values are ± the 95% confidence limit.

To assess whether the difference in enzyme efficiency is due to a difference in K_M or in k_{cat}, we carried out a full kinetic analysis on the 19-mer oligos shown in Table 1 using a fluorescence-based assay that has been shown to yield the same kinetic constants as radioactive assays (*32*). By varying the concentration of substrate DNA, we obtained the data shown in Figure 5, which were fit using standard Michaelis−Menten kinetics to determine K_M and k_{cat}. The kinetic parameters are summarized in Table 5. The K_M of UDG for the AUA/TPT sequence is more than 10-fold smaller than the K_M for the GUG/CPC sequence. UDG is inhibited by its tight binding to the product (*13*, *32*), and therefore product release is the rate-limiting step in catalysis by UDG. Under these conditions, K_M can be viewed as an apparent affinity constant. Accordingly, the recognition of uracil by UDG as expressed in the affinity of the enzyme to the DNA is better in the AUA/TPT context than in the GUG/CPC context. We observe that k_{cat} for the GUG/CPC sequence is approximately

two times greater than for the AUA/TPT sequence. This may be due to differential product release as UDG may bind more tightly to its product in the more flexible AUA/TPT sequence. As this paper was in preparation, a kinetic analysis of the HSV1 UDG on several sequences was reported by Bellamy and co-workers (*22*). In contrast to the studies reported here, they used a catalytically inactive UDG to demonstrate that the observed differences in UDG efficiency can be explained by differences in equilibrium binding. Although our sequences are not identical to those in the Bellamy paper, our results agree qualitatively. In both cases, A·T-rich regions surrounding the uracil yield better substrates than G·C-rich regions, and the differences in efficiency arise from differences in K_M.

In this work, we provide a detailed analysis of *local* differences in the DNA dynamical properties that account for the variations in UDG activity with DNA sequence. A combination of MD simulations and fluorescence spectroscopy illustrates key differences in the structure and dynamics of the two DNA sequences. The AUA/TAT sequence is more flexible and less stacked than the GUG/CAC sequence. Furthermore, we have shown a direct correlation between DNA flexibility and UDG activity for the sequences studied, consistent with our hypothesis.

Crystal structures of several other DNA repair enzymes in complex with DNA show that the DNA is severely distorted (*38*−*40*). DNA bending is energetically unfavorable, and thus a more flexible substrate will require less energy to bend and allow tighter binding by the enzyme. Repair enzymes having reduced affinities for rigid DNA with consequent lowered efficiency could lead to a greater frequency of mutations in these sequences. DNA flexibility could directly impact the efficiency of damaged DNA repair, since repair would depend on the context in which the damage occurs. Many other DNA binding proteins, including transcriptional regulators (*41*, *42*) and restriction enzymes (*43*, *44*), have been shown to bend their target DNA. Thus, we propose that DNA flexibility is important not only in the recognition of DNA damage but also in formation of other DNA−protein complexes.

ACKNOWLEDGMENT

We thank Dr. James T. Stivers (Johns Hopkins University) for providing us with the *E. coli* UDG expression system.

REFERENCES

1. Verri, A., Mazzarello, P., Biamonti, G., Spadari, S., and Focher, F. (1990) The specific binding of nuclear protein(s) to the cAMP responsive element (CRE) sequence (TGACGTCA) is reduced by the misincorporation of U and increased by the deamination of C, *Nucleic Acids Res. 18*, 5775−5780.
2. Kunkel, T. A., and Bebenek, K. (2000) DNA replication fidelity, *Annu. Rev. Biochem. 69*, 497−529.
3. Mosbaugh, D. W., and Bennett, S. E. (1994) Uracil-excision DNA repair, *Prog. Nucleic Acid Res. Mol. Biol. 48*, 315−370.
4. Mol, C. D., Parikh, S. S., Putnam, C. D., Lo, T. P., and Tainer, J. A. (1999) DNA repair mechanisms for the recognition and removal of damaged DNA bases, *Annu. Rev. Biophys. Biomol. Struct. 28*, 101−128.
5. Srivastava, D. K., Berg, B. J., Prasad, R., Molina, J. T., Beard, W. A., Tomkinson, A. E., and Wilson, S. H. (1998) Mammalian abasic site base excision repair. Identification of the reaction sequence and rate-determining steps, *J. Biol. Chem. 273*, 21203−21209.
6. Krokan, H., and Wittwer, C. U. (1981) Uracil DNA-glycosylase from HeLa cells: general properties, substrate specificity and effect of uracil analogues, *Nucleic Acids Res. 9*, 2599−2613.
7. Delort, A. M., Duplaa, A. M., Molko, D., Teoule, R., Leblanc, J. P., and Laval, J. (1985) Excision of uracil residues in DNA: mechanism of action of *Escherichia coli* and *Micrococcus luteus* uracil-DNA glycosylases, *Nucleic Acids Res. 13*, 319−335.
8. Savva, R., McAuley-Hecht, K., Brown, T., and Pearl, L. (1995) The structural basis of specific base-excision repair by uracil-DNA glycosylase, *Nature 373*, 487−493.
9. Xiao, G., Tordova, M., Jagadeesh, J., Drohat, A. C., Stivers, J. T., and Gilliland, G. L. (1999) Crystal structure of *Escherichia coli* uracil DNA glycosylase and its complexes with uracil and glycerol: structure and glycosylase mechanism revisited, *Proteins 35*, 13−24.
10. Pearl, L. H. (2000) Structure and function in the uracil-DNA glycosylase superfamily, *Mutat. Res. 460*, 165−181.
11. Slupphaug, G., Mol, C. D., Kavli, B., Arvai, A. S., Krokan, H. E., and Tainer, J. A. (1996) A nucleotide-flipping mechanism from the structure of human uracil-DNA glycosylase bound to DNA [see comments], *Nature 384*, 87−92.
12. Kavli, B., Slupphaug, G., Mol, C. D., Arvai, A. S., Peterson, S. B., Tainer, J. A., and Krokan, H. E. (1996) Excision of cytosine and thymine from DNA by mutants of human uracil-DNA glycosylase, *EMBO J. 15*, 3442−3447.
13. Parikh, S. S., Mol, C. D., Slupphaug, G., Bharati, S., Krokan, H. E., and Tainer, J. A. (1998) Base excision repair initiation revealed by crystal structures and binding kinetics of human uracil-DNA glycosylase with DNA, *EMBO J. 17*, 5214−5226.
14. Friedman, R. A., and Honig, B. (1995) A free energy analysis of nucleic acid base stacking in aqueous solution, *Biophys. J. 69*, 1528−1535.
15. Bloomfield, V. A., Crothers, D. M., and Tinoco, I. (2000) *Nucleic acids: structures, properties and functions*, University Science Books, Sausalito, CA.
16. Ramstein, J., and Lavery, R. (1988) Energetic coupling between DNA bending and base pair opening, *Proc. Natl. Acad. Sci. U.S.A. 85*, 7231−7235.
17. Fuxreiter, M., Luo, N., Jedlovszky, P., Simon, I., and Osman, R. (2002) Role of base flipping in specific recognition of damaged DNA by repair enzymes, *J. Mol. Biol.* (submitted for publication).
18. Rachofsky, E. L., Ross, J. B. A., and Osman, R. (2001) Conformation and dynamics of normal and damaged DNA, *Comb. Chem. High Throughput Screening 4*, 675−706.
19. Slupphaug, G., Eftedal, I., Kavli, B., Bharati, S., Helle, N. M., Haug, T., Levine, D. W., and Krokan, H. E. (1995) Properties of a recombinant human uracil-DNA glycosylase from the UNG gene and evidence that UNG encodes the major uracil-DNA glycosylase, *Biochemistry 34*, 128−138.
20. Nilsen, H., Yazdankhah, S. P., Eftedal, I., and Krokan, H. E. (1995) Sequence specificity for removal of uracil from U.A pairs and U.G mismatches by uracil-DNA glycosylase from *Escherichia coli*, and correlation with mutational hotspots, *FEBS Lett. 362*, 205−209.
21. Eftedal, I., Guddal, P. H., Slupphaug, G., Volden, G., and Krokan, H. E. (1993) Consensus sequences for good and poor removal of uracil from double stranded DNA by uracil-DNA glycosylase, *Nucleic Acids Res. 21*, 2095−2101.
22. Bellamy, S. R., and Baldwin, G. S. (2001) A kinetic analysis of substrate recognition by uracil-DNA glycosylase from herpes simplex virus type 1, *Nucleic Acids Res. 29*, 3857−3863.
23. Panayotou, G., Brown, T., Barlow, T., Pearl, L. H., and Savva, R. (1998) Direct measurement of the substrate preference of uracil-DNA glycosylase, *J. Biol. Chem. 273*, 45−50.
24. Case, D. A., Pearlman, D. A., Caldwell, J. W., Cheatham, T. E., III, Ross, W. S., Simmerling, C., Darden, T., Merz, K. M., Stanton, R. V., Cheng, A., Vincent, J. J., Crowley, M., Tsui, V., Radmer, R., Duan, Y., Pitera, J., Massova, I., Seibel, G. L., Singh, U. C., Weiner, P. K., and Kollman, P. A. (1999) *AMBER 6.0*, University of California, San Francisco.
25. Lavery, R., and Sklenar, H. (1988) The definition of generalized helicoidal parameters and of axis curvature for irregular nucleic acids, *J. Biomol. Struct. Dyn. 6*, 63−91.
26. Stivers, J. T., Pankiewicz, K. W., and Watanabe, K. A. (1999) Kinetic mechanism of damage site recognition and uracil flipping by Escherichia coli uracil DNA glycosylase, *Biochemistry 38*, 952−963.
27. Rachofsky, E. L., Seibert, E., Stivers, J. T., Osman, R., and Ross, J. B. A. (2001) Conformation and Dynamics of Abasic Sites in DNA Investigated by Time-Resolved Fluorescence of 2-Aminopurine, *Biochemistry 40*, 957−967.

28. Rachofsky, E. L., Osman, R., and Ross, J. B. A. (2001) Probing Structure and Dynamics of DNA with 2-Aminopurine: Effects of Local Environment on Fluorescence, *Biochemistry 40*, 946−956.
29. Grinvald, A., and Steinberg, I. Z. (1974) On the analysis of fluorescence decay kinetics by the method of least-squares, *Anal. Biochem. 59*, 583−598.
30. Bevington, P. R. (1969) *Data reduction for the physical sciences*, McGraw-Hill, New York.
31. Straume, M., Frasier-Cadoret, S. G., and Johnson, M. L. (1991) in *Topics in Fluorescence Spectroscopy* (Lakowicz, J. R., Ed.) pp 177−240, Plenum, New York.
32. Stivers, J. T. (1998) 2-Aminopurine fluorescence studies of base stacking interactions at abasic sites in DNA: metal-ion and base sequence effects, *Nucleic Acids Res. 26*, 3837−3844.
33. Lankaš, F., Šponer, J., Hobza, P., and Langowski, J. (2000) Sequence-dependent elastic properties of DNA, *J. Mol. Biol. 299*, 695−709.
34. Harrington, R. E. (1993) Studies of DNA bending and flexibility using gel electrophoresis, *Electrophoresis 14*, 732−746.
35. De Santis, P., Palleschi, A., and Savino, M. (1993) A simple physical model for the gel electrophoretic manifestations of sequence-dependent DNA superstructures, *Electrophoresis 14*, 699−703.
36. Jean, J. M., and Hall, K. B. (2001) 2-Aminopurine fluorescence quenching and lifetimes: role of base stacking, *Proc. Natl. Acad. Sci. U.S.A. 98*, 37−41.
37. Saenger, W. (1984) *Principles of Nucleic Acid Structure*, Springer-Verlag, New York.
38. Hosfield, D. J., Guan, Y., Haas, B. J., Cunningham, R. P., and Tainer, J. A. (1999) Structure of the DNA repair enzyme endonuclease IV and its DNA complex: double-nucleotide flipping at abasic sites and three-metal-ion catalysis, *Cell 98*, 397−408.
39. Hollis, T., Ichikawa, Y., and Ellenberger, T. (2000) DNA bending and a flip-out mechanism for base excision by the helix-hairpin-helix DNA glycosylase, *Escherichia coli* AlkA, *EMBO J. 19*, 758−766.
40. Vassylyev, D. G., Kashiwagi, T., Mikami, Y., Ariyoshi, M., Iwai, S., Ohtsuka, E., and Morikawa, K. (1995) Atomic model of a pyrimidine dimer excision repair enzyme complexed with a DNA substrate: structural basis for damaged DNA recognition, *Cell 83*, 773−782.
41. Kamada, K., Shu, F., Chen, H., Malik, S., Stelzer, G., Roeder, R. G., Meisterernst, M., and Burley, S. K. (2001) Crystal structure of negative cofactor 2 recognizing the TBP-DNA transcription complex, *Cell 106*, 71−81.
42. Bell, C. E., and Lewis, M. (2001) Crystallographic analysis of lac repressor bound to natural operator o1, *J. Mol. Biol. 312*, 921−926.
43. Horton, N. C., and Perona, J. J. (1998) Role of protein-induced bending in the specificity of DNA recognition: crystal structure of EcoRV endonuclease complexed with d(AAAGAT) + d(ATCTT), *J. Mol. Biol. 277*, 779−787.
44. Deibert, M., Grazulis, S., Janulaitis, A., Siksnys, V., and Huber, R. (1999) Crystal structure of MunI restriction endonuclease in complex with cognate DNA at 1.7 A resolution, *EMBO J. 18*, 5805−5816.

BI026121O